Structural and superconducting characteristics of $YBa_2Cu_3O_7$ films grown by Fluorine-Free Metal-Organic Deposition Route

Yue Zhao[a], Jingyuan Chu[a], Thomas Qureishy[b], Wei Wu[a], Zhiwei Zhang[a], Pavlo Mikheenko[b], Tom H. Johansen[b,c], Jean-Claude Grivel[d]

a School of Electronic Information and Electrical Engineering, Shanghai Jiao Tong University, 200240 Shanghai, China

b Department of Physics, University of Oslo, PO Box 1048 Blindern, 0316 Oslo, Norway.

c Institute for Superconducting and Electronic Materials, University of Wollongong, North Fields Avenue, Wollongong, NSW 2522, Australia

d Department of Energy Conversion and Storage, Technical University of Denmark,4000 Roskilde, Denmark

Abstract

Microstructure and superconducting performance of $YBa_2Cu_3O_7$ (YBCO) films deposited on $LaAlO_3$ single crystals (LAO) substrates by a fluorine-free metal-organic deposition (FF-MOD) technique, have been studied by means of X-ray reciprocal space mapping (RSM), cross-sectional transmission electron microscopy (TEM) and magneto-optical (MO) imaging.Combining the X-ray diffraction and the TEM cross-sectional analysis, it is revealed that stacking faults, i.e. $YBa_2Cu_4O_x$ intergrowths, and *ab*-plane twins are main defects in the FF-MOD YBCO films. Due to the highly epitaxial growth mechanism related to transient liquid phase, the LAO twinned substrate structure is also inherited in the FF-YBCO films. The low-density planar defects containing dislocations parallel to *c*-axis result in stripy patterns observed in the MO images. For comparison, the low-fluorine (LF) MOD film show a texture mosaic spread in the *ab* plane and is little influenced by the LAO twinning underneath, implying the severe structural disorder most likely associated with the large amount of small-angle grain boundaries. Moreover, the higher density of stacking faults was also detected by XRD θ–2θ scan in these films. It is suggested that associated partial dislocations formed at the boundary between the stacking faults and YBCO matrix act as strong linear (or dot) pinning centers. These structural characteristics are well in line with the better superconducting performance of the low fluorine-MOD film, in particular under

external magnetic field at 77 K. This work offers an in-depth insight into the correlation between the microstructure and superconductivity in the MOD YBCO films.

Keyword: superconducting films; epitaxial growth; metal-organic deposition; transmission electron microscopy; magneto-optical imaging

Correspondence should be addressed to Y. Zhao, e-mail: *yuezhao@sjtu.edu.cn*

1. Introduction

The second-generation superconducting tapes (2G HTS) based on $REBa_2Cu_3O_{7-\delta}$ films (REBCO, where RE is Y or rare earth element) have attracted a great deal of attention in the fields of power transmission cables, fault current limiters and rotary machines. The main challenge for practical applications in terms of materials science is industrial production of 2G HTS tapes with high current carrying capacity. For this, it is of great importance to comprehensively understand the correlation between the microstructure and superconducting properties of REBCO films. Several great advances have been achieved by tuning the microstructure of such superconducting films, such as by utilizing biaxially-textured substrates [1, 2] and introducing artificial pinning centers [3-5]. The microstructure modulation is still believed to be the most attractive strategy to further boost the superconducting performance of REBCO tapes.

It is well known that critical current density (J_c) in the superconducting layer is thickness-dependent, i.e., the J_c decreases dramatically as the film is grown thicker, while it also exhibits strong temperature and magnetic field dependence. Previous studies clearly demonstrated that both these issues are strongly associated with the vortex motion that dissipates energy and causes electrical resistance [6, 7]. Aiming at superior superconducting performance, it is necessary to deposit the REBCO films with high homogeneity on the macroscale but with desirable defect landscape on the nanoscale [8, 9]. Such combined microstructural features would allow carrying high J_c at the greatest level in the REBCO matrix, thus taking advantage of the fact that vortex motion is suppressed by the local defects [10]. Consequently, tailoring the microstructure by precise control of the nucleation and growth mechanism in REBCO films recently became a hot topic in the field. Several factors could strongly affect these processes, such as film/precursor composition [11-13], interface properties [14, 15], deposition techniques and processing parameters [16-18].

Among all the deposition techniques developed so far, chemical solution deposition is considered to be one of the most promising routes. It shows great potential of industrialization at low cost, while being capable of obtaining tunable microstructure. For the synthesis of YBCO films, a diversity of precursor solutions has been successfully developed [19]. Depending on the presence of fluorine, different chemical reaction mechanisms take place during YBCO conversion, consequently leading to distinguished microstructural characteristics in the final products. To date, researchers have carried out extensively studies on the trifluoroacetate metal organic deposition (TFA-MOD) route, during which

the correlation between the processing parameters and microstructure became much clearer [20, 21]. Furthermore, the formation of defects, including intrinsic, e.g., stacking faults (SFs) and extrinsic, e.g, , nano-inclusion, and their effects on the superconducting performance, especially on the J_c enhancement, have been illustrated [22-24].

In this paper, we perform a comprehensive study of the microstructural and superconducting characteristics of YBCO films, deposited by using a novel fluorine-free (FF) solution. The solution does not contain nitrogen-based chelating agents (i.e., ammonia or its derivatives, for example, triethanolamine) involved in the precursor solution synthesis. Therefore, the release of most likely toxic gases (i.e., nitrogen oxides) is in principle eliminated during the pyrolysis. In addition, because of the presence of a transient liquid phase during YBCO conversion, the process exhibits a super-fast growth rate compared with that of the conventional TFA-MOD route [25]. The main aim of the present study is to further understand the correlation between the defect structure and superconducting properties using X-ray reciprocal space mapping (RSM), transmission electron microscopy as well as the magneto-optical imaging technique. A comparative study between the films grown from FF- and low-fluorine (LF) solutions was also carried out systematically.

2. Material and methods

2.1 Solution synthesis and growth of YBCO films

YBCO films with thickness about 200 nm were synthesized by a FF-MOD route using propionic acid only as a solvent. The propionate-based precursor solutions and YBCO film itself were prepared following a procedure reported elsewhere [26]. In short, first, stoichiometric amounts (1:2:3) of Y, Ba and Cu acetates were simply mixed and dissolved in propionic acid in a flask. Second, the flask was sealed, and the mixture was heated at 80 °C under magnetic stirring, using a hotplate. After stirring for two hours, all the reagents were completely dissolved in the acid, and a dark-blue solution without any precipitation was obtained. To compensate the evaporation of solvent during the long-time heating, the total cation concentration in the solutions was adjusted to 1.5 M by adding a certain amount of propionic acid. 5 mm×5 mm (001) $LaAlO_3$ (LAO) single crystals (CrysTec GmbH) were used as substrate. Prior to coating, the substrates were cleaned with ethanol in an ultrasonic bath for 5 min and dried by using compressed air. A spin-coating was carried out under ambient conditions. The rotation speed in the process was set to 3000 rpm, and the dwelling time was 60 seconds. To convert the precursor to an YBCO phase, a typical three-step heat treatment process was applied in an

atmosphere-controlled tubular furnace. For comparison, an YBCO film deposited by a LF-MOD route was also prepared. The details of the procedure are described in Ref. [27].

2.2 YBCO structural characterization

The phase purity, crystallinity, global crystallographic texture and the reciprocal space maps of the YBCO films were studied using high resolution X-ray diffraction (XRD) with Cu K_α radiation (λ =1.54 Å) in a four-circle diffractometer (Rigaku, smartlab). Film morphology and film thickness were analyzed by a scanning electron microscope (SEM, Zeiss Supra 35) equipped with an inlens detector. Specimens for cross-sectional TEM observations were prepared by conventional routine including cutting, gluing, grinding, polishing, and final ion polishing. Special precautions were taken to minimize chemical reaction between the cooling media and YBCO phase during cutting and grinding. Selected-area electron diffraction (SAED) and TEM studies were performed using an aberration-corrected scanning transmission electron microscope (STEM, JEOL ARM 200CF) with a double-tilt holder and a cold field emission source operated at 200 kV. High angle annular dark-field (HAADF) imaging was carried out down to the atomic level to look for the presence of defects and possible second phases.

2.3 Superconducting properties characterization

The critical current density, J_c, was calculated based on the Bean model [28] using the opening of hysteresis loops obtained by a vibrating sample magnetometer (VSM) under magnetic field applied perpendicular to the plane of films. To analyze the current distribution and magnetic flux channeling effects in the YBCO films, magneto-optical imaging (MOI) technique was used. The MOI setup makes use of the Faraday effect in the magneto-optical layer (a ferrite garnet film [29, 30]), which is capable of achieving high magnetic sensitivity and desirable signal-noise characteristics [31]. In this work, the specimens for MOI were zero-field cooled (ZFC) to 20 K, then an external magnetic field was applied perpendicular to the plane of the film and increased to several tens of mT or until full penetration of magnetic flux from the edges of the sample.

3. Results and discussion

3.1 General comparison between the YBCO films grown by FF- and LF-MOD routes

First, two YBCO films with similar thicknesses (~200 nm) prepared by conventional FF-and LF- MOD were compared. Their key structural and superconducting parameters are shown in Table 1. It can be seen that both films are highly textured, and their intensity ratios of the YBCO (005) and (004)

reflections, which is smaller than 20 also suggests that the oxygen deficiency is smaller than 0.1 in both films. However, the FF-MOD YBCO film exhibits sharper in-plane and out-of-plane textures than the LF-MOD film, as evidenced by smaller FWHM values of YBCO (103) ϕ-scan and (005) rocking curve. This is probably related to enhanced transient liquid phase during YBCO conversion in the FF-MOD process, which is in agreement with the morphologic features discussed in the following. Superconducting transition temperature (T_c onset) determined by AC susceptibility measurements is around 90 K for both films, with a transition width of about 2 K. As shown in figure 1, the similar J_c *(B)* dependence behavior and comparable J_c values (above 3.5 MA/cm^2, at 77 K, s.f.) were observed for these films. However, B^* and F^{MAX} in the LF-MOD YBCO film are higher than those in the FF-MOD one. It is known that B^* is often associated with a single-pinning regime in the low field, while the α parameter in $J_c\ (H) \propto H^{-\alpha}$ corresponds to a collective interaction regime of vortices in the medium fields range. Therefore, we can conclude that better superconducting properties in external magnetic fields are obtained in the LF-MOD YBCO film.

3.2 Detailed structural characterization of the YBCO films

To shed light on the differences in microstructure and superconducting properties of the films, detailed XRD, SEM and TEM characterizations were performed. In the XRD θ–2θ scans (figure 2), besides sharp (00*l*) YBCO peaks, asymmetric peak broadening of the (001), (002) and (004) reflections (pointed by arrows in the XRD patterns) is also clearly observed in both films. Such peak broadening is an indication of the presence of $YBa_2Cu_4O_x$ (Y124-type intergrowths) [32]. Furthermore, the more significant peak broadening in the LF-MOD film suggests that a larger amount of the Y124 intergrowths are present in this case. In the YBCO (001) reciprocal space maps (RSM) (inset in figure 2, lower panel), one can further identify the out-of-plane texture components and the epitaxial relationship between the Y124 intergrowth–and YBCO matrix, i.e., the 124-phase forms a laminar structure well-orientated along the *ab*-plane. In SEM images (figure 3), both films show a homogeneous microstructure at the macro-scale with a small amount of *a*-axis oriented grains. However, one can notice that there is a significant difference between the FF- and LF-MOD YBCO films at sub-micrometre scale. Void-free and much smoother morphology is observed on the FF-MOD YBCO film surface. Plate-like grains with large in-plane grain size and meandering grain boundaries appear, being indicative of formation of an enhanced liquid phase. Such topographic features provide

clear evidence of completely different growth mechanism in these two chemical solution deposition routes.

Secondly, YBCO (103) RSMs (figure 4) reveal the epitaxial relationship between the LAO substrate and the YBCO films. More than one sharp peak is observed at high Q_z positions, revealing small in-plane misoriented LAO (100) and (110) twins. This phenomenon is related to a second-order phase transition in the LAO material [33]. Normally, the LAO twinning has little effect on the YBCO film growth, which is also obviously valid for the LF-MOD YBCO film. Namely, the YBCO (103) reflection in the film shows much broader than in the LAO (110). There is no clear sign of YBCO grains copying the features of LAO twinning underneath. In contrast with the LF-MOD YBCO film, the YBCO peak splitting is observed in the FF-MOD sample, which is associated with *ab* twinning in the YBCO matrix due to the tetragonal-orthorhombic phase transition during oxygenation process [34]. By carefully checking the YBCO(103) ϕ–scan (not shown), it is found that two peaks are separated by 0.9° with respect of each other, suggesting a superior crystal structure quality ~~in~~ of the FF-MOD YBCO film.

Furthermore, cross-sectional TEM study reveals more structural details of the FF-YBCO matrix and the YBCO/LAO interface. Figure 5 a) and b) show representative cross-sectional low-magnification overview TEM image and the corresponding SAED pattern. Good crystallinity and high texture quality were confirmed by the SAED pattern. In addition, the film matrix exhibits a rather dense and void-free microstructure, which is in line with the surface morphologic observations with SEM. A large amount of bright and dark columns with spacing of 20-30 nm is also seen through the film thickness. Most of the columns are separated by bright lines parallel to the *ab*-plane (pointed by yellow arrows). This feature corresponds to grain mis-orientations in the *ab* plane, while the bright lines show stacking faults. Both features are similar to those reported by other researchers [35, 36].

To reveal the heterogeneous interface structure at the atomic level, HAADF images were taken by TEM. They are shown in figure 6, in which the image brightness is proportional to Z^n (Z is the average atomic number along the column of the scanned crystal, and n=1.5-2) [37]. The cation sublattice in the YBCO and LAO was identified and superimposed on the image. At the interface (figure 6a), it is seen that the YBCO structure cube-on-cube grows on the LAO substrate, i.e., $(100)_{\text{pseudo-perovskite}}$. The LaO plane is the terminating layer of the LAO substrate in this study, while the CuO plane in the YBCO is in contact with the substrate's LaO plane. It appears that the reaction/diffusion is negligible and an

initial perfect 2D growth of YBCO takes place at the interface. The YBCO/LAO interface stacking sequences is identified as BaO-CuO_2-Y-CuO_2-(BaO-CuO-LaO)-AlO_2. Such observation is in agreement with previous studies [38, 39], confirming that CuO plane is the starting atomic plane at the YBCO/LAO interface. One should notice, however, that although the nucleation and growth mechanism for chemical solution deposition routes (*in-situ*) differs completely from that of physical vapor deposition routes (*ex-situ*), the formation of the interface stacking sequences is the same, seemingly being governed by the substrate structure. This implies that the intermediate phase has little influence on the stacking sequences at the FF-MOD YBCO/LAO interface after structure re-organization triggered by the transient liquid phase. Figure 6b confirms that the planar defects present as bright lines in the low magnification TEM image consist of two sequential CuO planes corresponding to the $YBa_2Cu_4O_8$ (Y124) phase. This feature is spread through the thickness.

To illustrate the interface mismatch and strain relaxation, filtered fast Fourier transformation on the HAADF images was performed, and Bragg mask was applied to guide the eye as shown in figure 7. Considering that the in-plane lattice mismatch for YBCO (orthorhombic) is -1.57 %, the misfit dislocation spacing is 12.16 nm as calculated by using $d_{002s}*d_{002f} / |d_{002s}-d_{002f}$. Experimentally, misfit dislocation spacing (region I and II) does not match the calculated value. Anothe region (III) with different type of dislocation is also observed. The discrepancy implies rather a complex stress relaxation mechanism during the formation of YBCO. It is interesting to notice that highly-strained YBCO layer at interface is only about 1-2 nm thick (only one or two unit cells), which is thinner than interface layer reported by other researchers [40]. Besides, we also observed very few Y_2O_3 particles close to the interface but separated from it by a thin YBCO layer, as shown in figure 8. It is known that Y_2O_3 is one of the main intermediate phases formed after decomposition of precursor, which is consumed by the reaction with the Ba-Cu-O liquid phase at the last step of YBCO formation [26]. One can see that Y_2O_3 inclusion keeps the same crystallographic orientation with respect to YBCO, i.e, (001)[110] Y_2O_3// (001)[100]YBCO, probably due to the close lattice parameters in this constitution. However, certain amounts of stacking faults were initiated by the Y_2O_3-YBCO interface, being related to the accommodation of the internal strain. Compared to other strong artificial pinning, such as $BaMO_3$ (M=Zr, Hf, etc), the lattice disorder at the interface of Y_2O_3 and YBCO in the FF film is very minor, and the density of the SFs is much lower.

3.3 Defects and flux pinning characterized by magneto-optical imaging technique

Magneto-optical images of both FF and LF films under different applied external fields at 20 K are shown in figure 9. ~~Typical flux penetration patterns are in the form of 'fingers' growing from the edges of the films.~~ The flux fronts enter the samples from the edges as the applied field is increased. In addition, one can see several defects that strongly distort ideal penetration at the corners and edges. In the FF-MOD YBCO film, needle-like stripes in two orthogonal directions were developed from three edges, i.e. horizontal stripes from both vertical edges, and vertical stripes from the bottom edge. As shown in figure 9, a domain-like structure is also observed in the image of the FF MOD film. Clearly, the feature is a consequence of the twinning in the LAO substrate. Since LAO is neither superconducting nor magnetic, the feature in the MO image exclusively belongs to the FF-MOD YBCO film. Such a striking feature is due to the stripy modulation of magnetic flux, which results from the YBCO domains inherited from the LAO twin grains along the *c*-axis [Qureishy et al., AML 8 1204 (2017)]. However, the LF-YBCO film grown on a similar LAO substrate (also with twins) shows normal flux penetration behaviour without stripes.

SFs and grain boundaries (including twin GBs, 90º and small angle GBs, <5 º, etc.) are typical defects in YBCO films prepared by various MOD routes. It is believed that SFs and associated dislocations have a strong influence on flux pinning. Based on our results, it seems that there are two important structural differences between the FF- and LF- YBCO films, as illustrated in figure 10. The main difference between them is in the density of the SFs. According to XRD, high density of SFs is present in the LF- YBCO films, which leads to strong flux pinning in magnetic field. Although SFs are planar defects parallel to *ab*-plane, which are expected to be effective only when H//ab, it is worth pointing out that partial dislocations formed at the boundary between the SFs and YBCO matrix may also act as point pinning centers when the magnetic field is away from the *ab*-planes [41]. Several other experimental studies also confirmed the pinning effect of SFs and associated dislocations on the superconductivity in YBCO films prepared by different techniques (MOD, PLD) [42, 43]. In addition to SFs, there are grain boundaries (GBs) acting as planar defects parallel to the *c*-axis, and they should also be taken into consideration. In the FF MOD films, there are several types of boundaries present in the films, among them twin GBs and domain boundaries initiated from LAO substrate. However, both of them have very low density, as evidenced by the XRD reciprocal space maps. Contrary to that, the relatively large FWHM value of the YBCO (103) ϕ–scan and (005) rocking curve reveal that a large

amount of low-angle grain boundaries is present in LF-MOD YBCO films. As a result, LF-YBCO films exhibit better pinning than FF-YBCO films.

4. Conclusion

A comprehensive study of microstructure and superconducting properties was carried out on YBCO films deposited on LAO single-crystalline substrates by FF- and LF- MOD routs. Both films show high J_c values close to 4 MA/cm^2 at 77 K, self-field, but demonstrate different superconducting performance in external magnetic fields. XRD and TEM analysis revealed that the grain boundaries, stacking faults and associated dislocations are the main defects providing high value of J_c. Severe structural disorder and high density of SFs associated with specific nucleation and growth mechanism were observed in the LF-YBCO films. Although the sharper in-plane and out-of-plane texture was obtained in the FF-YBCO films, the present twins and domain boundaries inherited from the LAO substrate are weak planar defects. HRTEM studies at the film-substrate interface revealed that CuO plane is in contact with LaO terminating plane of the substrate. At the interface, various types of dislocations and defects are found. However, highly strained region is only 1-2 nm thick. High resolution MO images reveal that the twins of LAO are transferred to the FF-YBCO film resulting in abnormal stripy modulation of magnetic flux.

Acknowledgements

The authors from Shanghai Jiao Tong University would like to acknowledge financial support from Science and technology committee of Shanghai Municipal under Grant 16521108300, National Key Research and Development Program 2017YFB0902300.

References

[1] Goyal, A, et al. "High critical current density superconducting tapes by epitaxial deposition of $YBa_2Cu_3O_x$, thick films on biaxially textured metals." Applied Physics Letters 69.12(1996):1795-1797.

[2] Iijima, Y., et al. "In-plane aligned $YBa_2Cu_3O_{7-x}$ thin films deposited on polycrystalline metallic substrates." Applied Physics Letters 60.6(1992):769-771.

[3] Kang, S., et al. "High-performance high-T_c superconducting wires. " Science 311.5769(2006):1911-4.

[4] Macmanus-Driscoll, J L, et al. Strongly enhanced current densities in superconducting coated conductors of $YBa_2Cu_3O_{7-x}$+$BaZrO_3$. ~~Nature Mater. 3, 439-443.~~" Nature Materials 3.7(2004):439-443.

[5] Bretos, Iñigo, et al. "Solution-derived $YBa_2Cu_3O_{7-\delta}$ (YBCO) superconducting films with $BaZrO_3$ (BZO) nanodots based on reverse micelle stabilized nanoparticles." Journal of Materials Chemistry C 3.16(2015):3971-3979.

[6] Claus, H., et al. "The "90 K" plateau of oxygen deficient $YBa_2Cu_3O_{7-\delta}$, single crystals." Physica C Superconductivity 198.1–2(1992):42-46.

[7] Senatore, Carmine, et al. "Field and temperature scaling of the critical current density in commercial REBCO coated conductors." Superconductor Science & Technology 29.1(2016):014002.

[8] Foltyn, S. R., et al. "Materials science challenges for high-temperature superconducting wire." Nature Materials 6.9(2007):631.

[9] Matsumoto, , et al. "Artificial pinning center technology to enhance vortex pinning in YBCO coated conductors." Superconductor Science Technology 23.1(2009):014001.

[10] Larbalestier, D, et al. "High-Tc superconducting materials for electric power applications." Nature 414.6861(2001):368.

[11] Gutiérrez, J, et al. "Strong isotropic flux pinning in solution-derived $YBa_2Cu_3O_{7-x}$ nanocomposite superconductor films." Nature Materials 6.5(2007):367-73.

[12] Engel, S., et al. "Enhanced flux pinning in $YBa_2Cu_3O_7$ layers by the formation of nanosized $BaHfO_3$ precipitates using the chemical deposition method." Applied Physics Letters 90.10(2007):052503.

[13] Erbe, Manuela, et al. "Improved $REBa_2Cu_3O_{7-x}$ (RE = Y, Gd) structure and superconducting properties by addition of acetylacetone in TFA-MOD precursor solutions." Journal of Materials Chemistry A 2.14(2014):4932-4944.

[14] Cantoni, C, et al. "Strain-driven oxygen deficiency in self-assembled, nanostructured, composite oxide films. " Acs Nano 5.6(2011):4783.

[15] Bian, Weibai, et al. "Manipulation of YBCO film properties by the introduction of perovskite

Formatted: English (U.K.)

$BaTiO_3$, nanodots as substrate decorations." Journal of the European Ceramic Society 36.14(2016):3417-3422.

[16] Kim, Ho Sup, et al. "Ultra-High Performance, High-Temperature Superconducting Wires via Cost-Effective, Scalable, Co-Evaporation Process." Scientific Reports 4.16(2014):4744.

[17] Bruno, A., et al. "Reducing intrinsic loss in superconducting resonators by surface treatment and deep etching of silicon substrates." Applied Physics Letters 106.18 (2015): 182601.

[18] Lee, Y., et al. "In-field performances of commercial REBCO tapes below liquid nitrogen temperatures." Physica C Superconductivity ~~495.~~495(2013):141-145.

[19] Zhao, Y., et al. "Comparison study of $YBa_2Cu_3O_{7-x}$ films deposited by using various carboxylate solutions." IEEE Trans. Appl. Supercond. 25 (2015): 6600204.

[20] Solovyov, Vyacheslav, Ivo K. Dimitrov, and Qiang Li. "Growth of thick $YBa_2Cu_3O_7$ layers via a barium fluoride process." Superconductor Science and Technology 26.1 (2012): 013001.

[21] Gazquez, J., et al. "Precursor Evolution and Nucleation Mechanism of $YBa_2Cu_3O_x$ Films by TFA Metal− Organic Decomposition." Chemistry of materials 18.26 (2006): 6211-6219.

[22] Gutierrez, J., et al. "The role of stacking faults in the critical current density of MOD films through a thickness dependence study." Superconductor Science and Technology 22.1 (2008): 015022.

[23] Guzman, Roger, et al. "Strain-driven broken twin boundary coherence in $YBa_2Cu_3O_{7-\delta}$ nanocomposite thin films." Applied Physics Letters 102.8 (2013): 081906.

[24] Holesinger, Terry G., et al. "Progress in Nanoengineered Microstructures for Tunable High-Current, High-Temperature Superconducting Wires." Advanced Materials 20.3 (2008): 391-407.

[25] Matsui, H., et al. "Reduced crystallization time of YBCO in a fluorine-free MOD process using uv-lamp irradiation." Physica C: Superconductivity and its applications 471.21 (2011): 960-962.

[26] Zhao, Yue, et al. "Growth of Highly Epitaxial $YBa_2Cu_3O_{7-\delta}$ Films from a Simple Propionate-Based Solution." Inorganic chemistry 54.21 (2015): 10232-10238.

[27] Zhao, Yue, et al. "Epitaxial growth of $YBa_2Cu_3O_{7-x}$ films on $Ce_{0.9}La_{0.1}O_{2-y}$ buffered yttria-stabilized zirconia substrates by an all-chemical-solution route." Cryst. Eng. Comm. 16.21 (2014): 4369-4372.

[28] Johansen and Bratsberg, “Critical-state magnetization of type-II superconductors in rectangular

slab and cylindrical geometries." J. Appl. Phys., 77(1995)3945–3952.

[29] L E Helseth, et al. "Faraday rotation spectra of bismuth-substituted ferrite garnet films with in-plane magnetization." Phys. Rev. B 64 (2001) 174406.

[30] L E Helseth, et al. "Faraday rotation and sensitivity of (100) bismuth-substituted ferrite garnet films." Phys. Rev. B 66 (2002) 064405.

[31] Ch Jooss, et al. "Magneto-optical studies of current distributions in high-Tc superconductors." Reports on Progress in Physics, 65(5) (2002) 651.

[32] Specht, Eliot D., et al. "Stacking faults in $YBa_2Cu_3O_{7-x}$: Measurement using x-ray diffraction and effects on critical current." Applied physics letters 89.16 (2006): 162510.

[33] Ye, Zu-Xin, et al. "Enhanced flux pinning in $YBa_2Cu_3O_{7-\delta}$ films by nanoscaled substrate surface roughness." Applied Physics Letters 87.12 (2005): 122502.

[34] Westerheim, A. C, et al. "Relation between electrical properties and microstructure of $YBa_2Cu_3O_{7-x}$ thin films deposited by single-target off-axis sputtering." Journal of Applied Physics 75.1(1994):393-403.

[35] Yamaguchi, I., et al. "Microstructural observations of epitaxial Y123 films on CeO_2-buffered sapphire by metal organic deposition." Journal of Physics: Conference Series. Vol. 43. No. 1. IOP Publishing, 2006.

[36] Sohma, M., et al. "Structural aspect of high-J_c MOD-YBCO films prepared on large area CeO_2-buffered YSZ substrates." Journal of Physics: Conference Series. Vol. 43. No. 1. IOP Publishing, 2006.

[37] Klenov, Dmitri O., and Susanne Stemmer. "Contributions to the contrast in experimental high-angle annular dark-field images." Ultramicroscopy 106.10 (2006): 889-901.

[38] Basu, S. N., A. H. Carim, and T. E. Mitchell. "A TEM study of microstructures of $YBa_2Cu_3O_{7-x}$ thin films deposited on $LaAlO_3$ by laser ablation." Journal of materials research 6.9 (1991): 1823-1828.

[39] Zhu, Yuanyuan, Chen-Fong Tsai, and Haiyan Wang. "Atomic interface sequence, misfit strain relaxation and intrinsic flux-pinning defects in different $YBa_2Cu_3O_{7-\delta}$ heterogeneous systems." Superconductor Science and Technology 26.2 (2012): 025009.

[40] Gàzquez, Jaume. "TEM investigation of growth mechanisms and microstructure of model YBCO

Formatted: Danish

Formatted: Danish

coated conductor architectures deposited by metalorganic decomposition." Tdx (2007).

[41] Yamasaki, H., et al. "Strong flux pinning due to dislocations associated with stacking faults in $YBa_2Cu_3O_{7-\delta}$ thin films prepared by fluorine-free metal organic deposition." Superconductor Science and Technology 23.10 (2010): 105004.

[42] Coll, M., et al. "Stress-induced spontaneous dewetting of heteroepitaxial $YBa_2Cu_3O_{7-x}$, thin films." Phys.Rev.B 73.7(2006):5420(1-8).

[43] Yamada, H, et al. "Flux pinning centres correlated along the c-axis in PLD-YBCO films." Superconductor Science & Technology 17.1(2003):58.

Figure and table captions

Table 1 Structural and superconducting parameters ~~performance~~ of the YBCO films. Here B* is a characteristic field determined by the criterion $J_c\ (B^*)/\ J_c\ (0)$=0.9. Parameter α is calculated by fitting $J_c\ (H)$ to a power-law dependence $J_c\ (H) \propto H^{-\alpha}$. F^{MAX} is the peak value of the pinning force (F_p) calculated from $J_c \times B$ as function of B at temperature of 77 K.

Fig. 1. Log–log scale $J_c\ (B)$ dependence (H//c) at temperature of 77 K for the LF- and FF-MOD YBCO films.

Fig. 2. XRD θ–2θ scans for LF- and FF-MOD YBCO films. The inset shows the YBCO (103) reciprocal space maps for these films.

Fig. 3. SEM image of the LF-MOD (a) and the FF-MOD (b) films. The arrows in the images point to *a*-axis grains.

Fig. 4. YBCO (103) reciprocal space maps (RSM) of the LF- and FF-MOD YBCO films. The diffractions from the LAO (110) and YBCO (103)/(013) peaks are pointed by arrows.

Fig. 5. Low-magnification cross-sectional TEM image and corresponding selected area electron diffraction patterns of the FF-YBCO film. In the TEM image, the *ab*-plane twin boundaries and stacking faults are pointed by the yellow and white arrows, respectively. All the diffraction spots are identified, and the orientation relationship between the film and substrate is ~~also~~ determined and shown in the figure.

Fig. 6. ~~HADDF~~ HAADF image of YBCO-LAO interface along <100> direction. The dark strips parallel to the interface are stacking faults pointed by the white arrows. Several typical regions (I, II and III) with different density of dislocations are found by (020) Bragg vector analysis.

Fig. 7. ~~HADDF~~ HAADF images superimposed with the YBCO, LAO and Y124 lattices at the YBCO/LAO interface (a) and in the YBCO matrix with a stacking fault (b). Both images are along the <100> axis.

Fig. 8. Cross-sectional TEM image of an area with an Y_2O_3 inclusion in the FF-MOD YBCO film.

Fig. 9. MO images of FF- and LF-MOD YBCO films in the upper and ~~lower~~ middle panel, respectively. In both cases, the films were zero-field-cooled to 20 K and a magnetic field was subsequently applied whose value is shown in the corner of each image. Areas in the blue squares are shown enlarged in the lower panel.

Fig. 10. Illustration of various defects in the YBCO films prepared by different MOD techniques. Note that all the defects are of nanometer-size level, except domain boundaries and voids.

Figures and tables

Table 1

sample	LF-MOD YBCO	FF-MOD YBCO
FWHM of YBCO (103) ϕ–scan	1.4º	~0.6º
FWHM of YBCO (005) rocking curve	0.8º	~0.15º
I(005)/I(004)	14	13.6
Tc (K)	~90 K	~90 K
ΔTc (K)	~2 K	~2 K
B^* (mT, at 77 K)	11.5	3.3
α (at 77 K)	-0.58	-0.56
F^{MAX}	3.2	2.0
J_c (MA/cm^2, at 77 K, s.f.)	3.9	3.7

Fig. 1

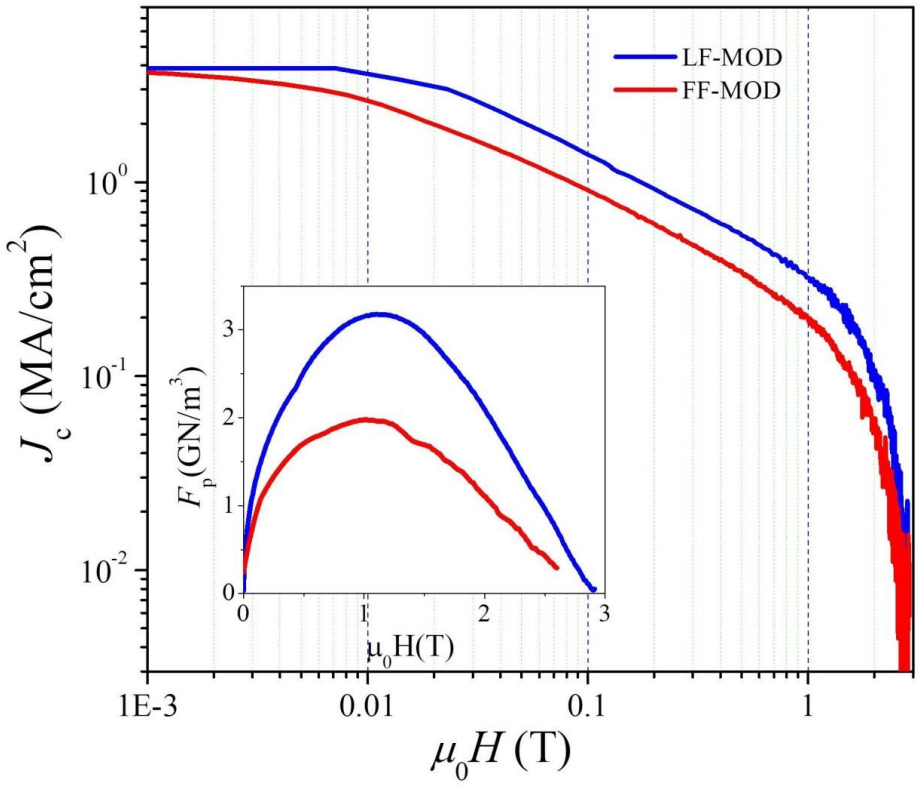
LF-MOD
FF-MOD
J_c (MA/cm^2)
10^0
10^{-1}
10^{-2}
1E-3
0.01
0.1
1
$\mu_0 H$ (T)
F_p (GN/m^3)
0
1
2
3
μ_0H(T)

Fig. 2

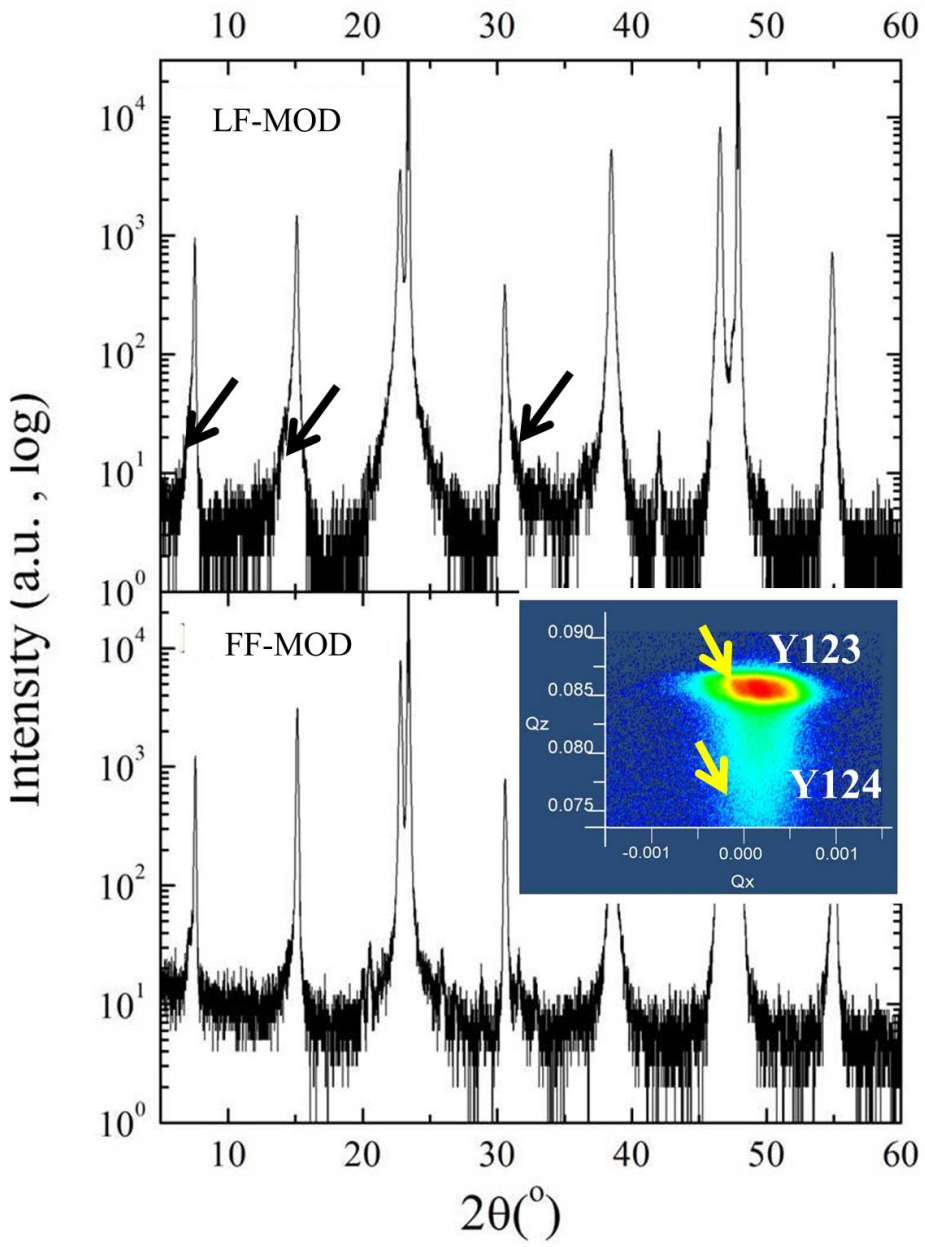
LF-MOD
FF-MOD
Intensity (a.u. , log)
2θ(°)
Y123
Y124
Qz
Qx
0.090
0.085
0.080
0.075
-0.001
0.000
0.001

Fig. 3

a）

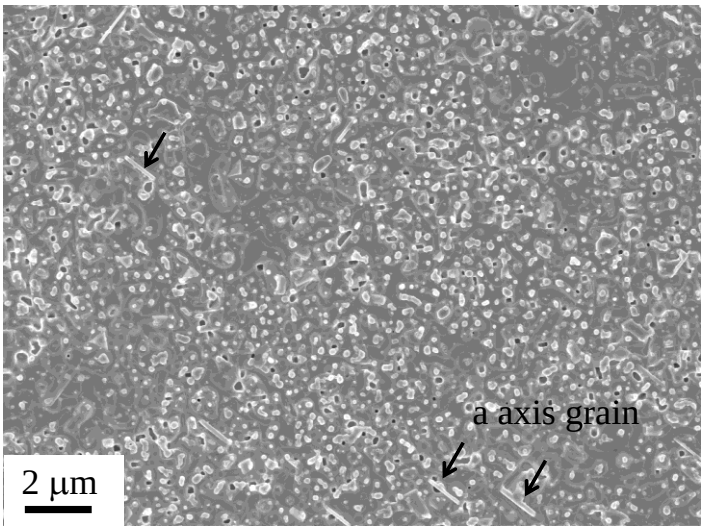

b）

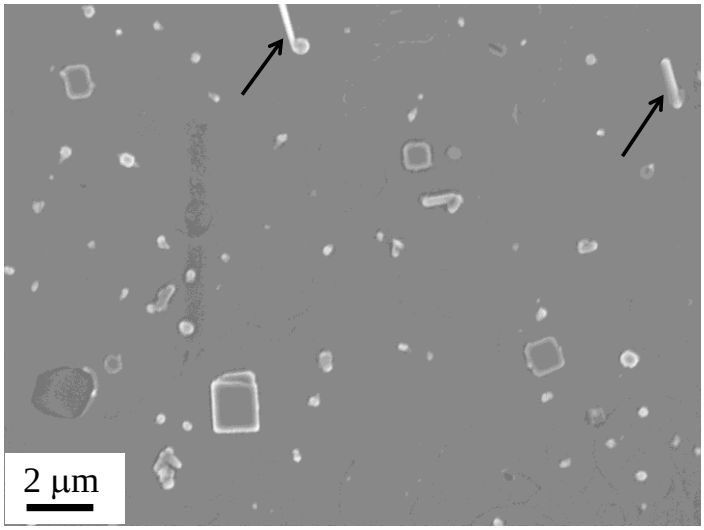

Fig. 4

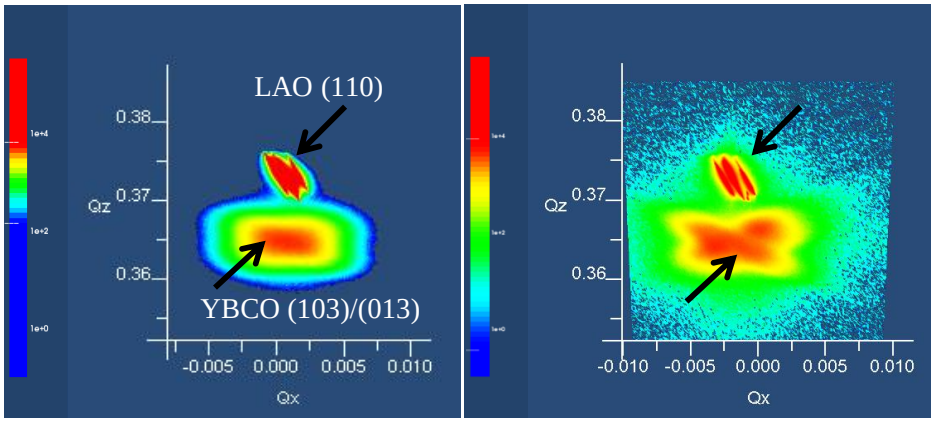
LAO (110)
YBCO (103)/(013)
Qz
Qx
0.38
0.37
0.36
-0.005
0.000
0.005
0.010
-0.010

Fig. 5

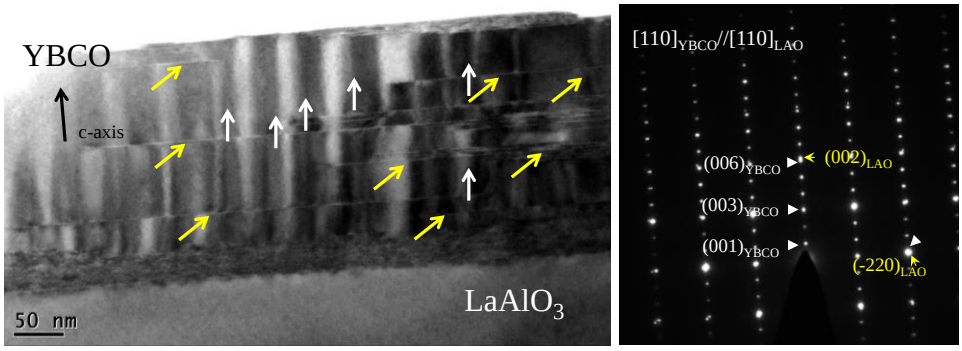
YBCO
c-axis
50 nm
LaAlO3
[110]YBCO//[110]LAO
(006)YBCO
(002)LAO
(003)YBCO
(001)YBCO
(-220)LAO

Fig. 6

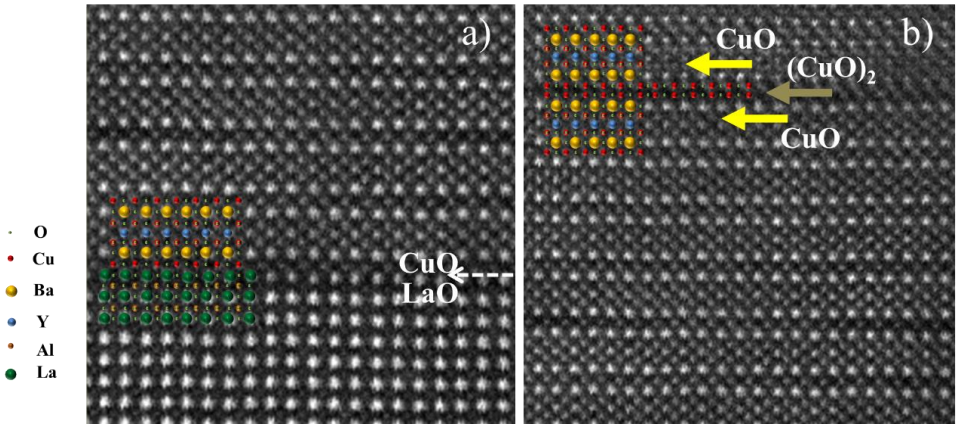

Fig. 7

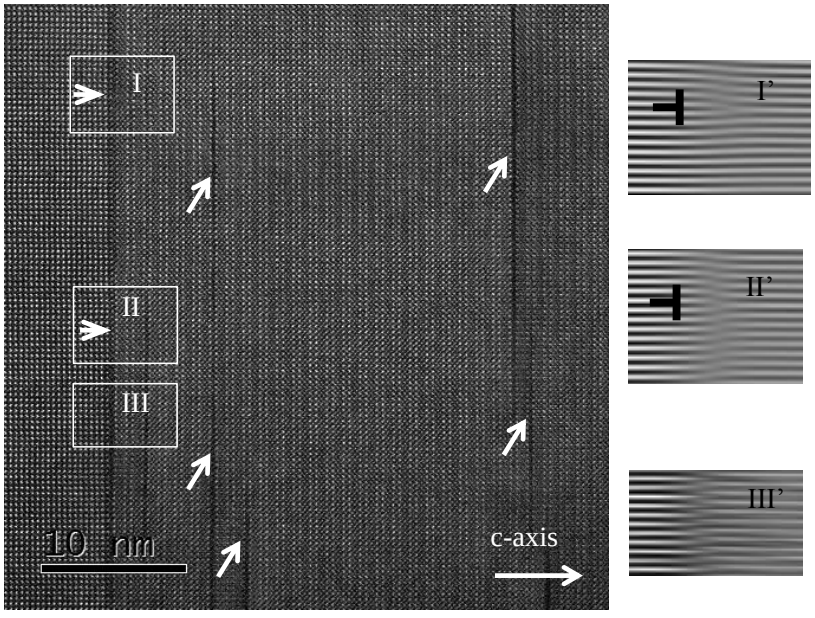

Fig. 8

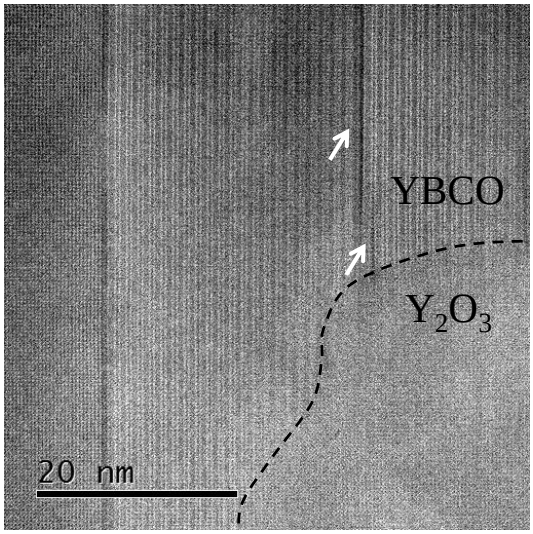
YBCO
Y_2O_3
20 nm

Fig. 9

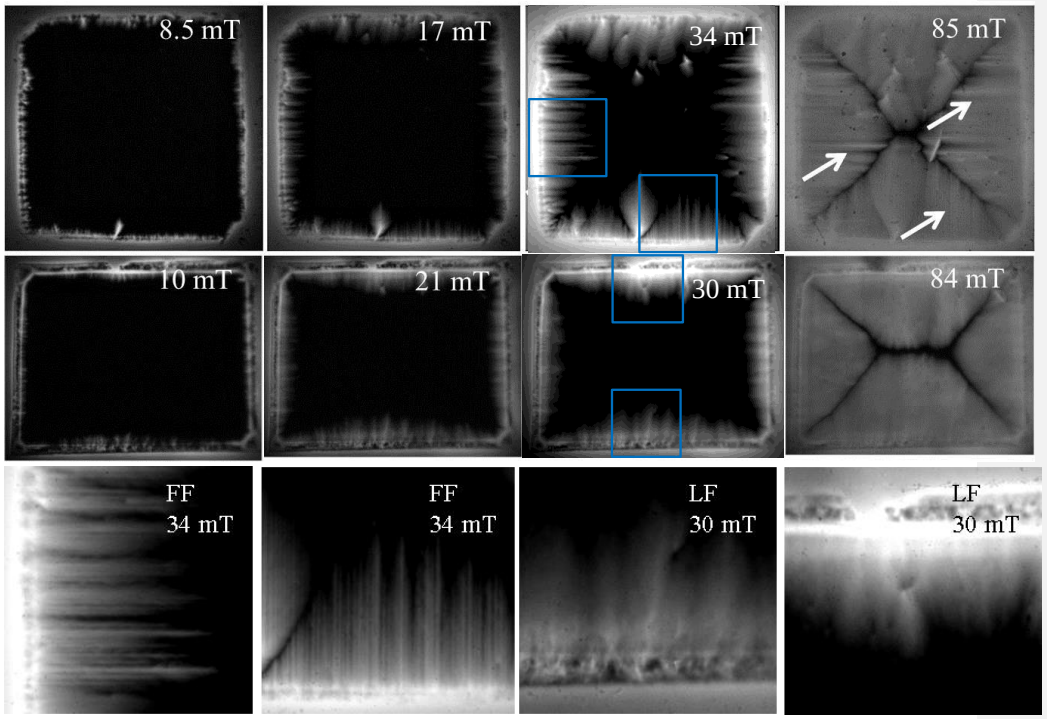
8.5 mT
17 mT
34 mT
85 mT
10 mT
21 mT
30 mT
84 mT
FF
34 mT
FF
34 mT
LF
30 mT
LF
30 mT

Fig. 10

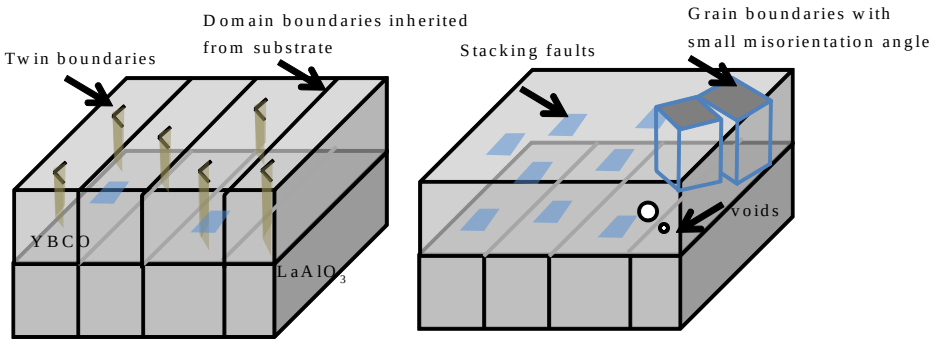

fluorine-free metal-organic deposition

low fluorine metal-organic deposition